Anisotropy of ferromagnetism in Co-implanted rutile

2005 J. Phys.: Condens. Matter 17 L359

(http://iopscience.iop.org/0953-8984/17/34/L01)

INSTITUTE OF PHYSICS PUBLISHING JOURNAL OF PHYSICS: CONDENSED MATTER

J. Phys.: Condens. Matter **17** (2005) L359–L366 doi:10.1088/0953-8984/17/34/L01

LETTER TO THE EDITOR

Anisotropy of ferromagnetism in Co-implanted rutile

N Akdogan[1,2], B Z Rameev[1,3], L Dorosinsky[4], H Sozeri[4], R I Khaibullin[3], B Aktaş[1], L R Tagirov[3,5,6], A Westphalen[2] and H Zabel[2]

[1] Gebze Institute of Technology, 41400 Gebze-Kocaeli, Turkey
[2] Institute für Experimentalphysik/Festkörperphysik, Ruhr-Universität Bochum, D-44780 Bochum, Germany
[3] Kazan Physical-Technical Institute of RAS, 420029 Kazan, Russia
[4] TUBITAK-UME (National Metrology Institute), PK 54, 41470 Gebze-Kocaeli, Turkey
[5] Kazan State University, 420008 Kazan, Russia

E-mail: Lenar.Tagirov@ksu.ru

Received 18 July 2005
Published 12 August 2005
Online at stacks.iop.org/JPhysCM/17/L359

Abstract

Magnetic anisotropy of cobalt implanted single-crystalline rutile has been studied by means of magneto-optical Kerr effect (MOKE) and superconducting quantum interference device (SQUID) techniques. We observed for the first time strong angular dependence of the remanent magnetization and coercive field in the plane of the implanted surface: twofold anisotropy for the (100)-substrate and fourfold anisotropy for the (001)-substrate samples. The observation opens up new possibilities to tailor magnetic anisotropies of the material. Possible origins of ferromagnetism and anisotropies in dielectric and diamagnetic single-crystalline TiO_2 samples after Co-ion implantation are discussed.

1. Introduction

Rapid progress in electronic devices that incorporate not only charge but also spin of electrons is the subject for a new branch of electronics, so-called spintronics [1–3]. The key problem in development of such devices is efficiency of injection of the spin-polarized current from a ferromagnetic material into a semiconductor. Due to the well known problem of a resistance mismatch at metal/semiconductor interfaces, hindering an effective spin injection [4], much is now concentrated on the development of room-temperature 'ferromagnetic semiconductors', such as Mn-doped Ga(In)As, MnGe [2, 3], and Co-doped ZnO [3, 5]. In this respect, recent observations of room-temperature ferromagnetism in Co-doped TiO_2 have attracted considerable attention to titanium dioxide as a host material for magnetic doping [6–11].

[6] Author to whom any correspondence should be addressed.

Optical transparency to visible light and very high refractive index make TiO_2 a superior candidate for magneto-optic applications.

Recently, we observed that single-crystalline rutile heavily implanted by Co ions shows very-high-Curie-temperature ferromagnetism [12]. We measured the saturation magnetization, its temperature dependence and the coercive field of our samples. However, the in-plane anisotropy, which is important for spintronic applications, has not been investigated. In this work we report for the first time on the strong influence that the crystallographic orientation of the substrate has on the magnetic anisotropy of single-crystalline TiO_2 (rutile structure) heavily implanted by Co ions. The in-plane anisotropies of the (100) and (001) samples have been studied by magneto-optical Kerr effect (MOKE) and superconducting quantum interference device (SQUID) techniques.

2. Sample preparation and experimental techniques

The substrates were $10 \times 10 \times 0.5$ mm^3 single-crystalline rutile plates which have been implanted in the *ILU*-3 ion accelerator (KPTI of RAS) with 40 keV Co^+ ions to a dose of 2×10^{17} ions cm^{-2} at an ion current density of 8–9 μA cm^{-2}. The sample holder was water cooled during the implantation to prevent the samples from overheating. The (100)- and (001)-face rutile plates were irradiated in a single run. The implanted plates were cut by a diamond cutter into smaller pieces for structural and magnetic studies.

Hysteresis loops were recorded using a high-resolution MOKE set-up in the longitudinal configuration with s-polarized light, which is well suited for measuring the Kerr angle as a function of the applied magnetic field. More details of the MOKE experimental set-up can be found in [13]. The experimental set-up allows for a rotation of the sample around its surface normal (by the angle φ) in order to apply a magnetic field in various in-plane directions and provide information about the in-plane magnetic anisotropy. Low-temperature magnetization hysteresis measurements were carried out using a Quantum Design MPMS XL SQUID magnetometer.

3. Experimental results

3.1. MOKE measurements

The left-hand column in figure 1 shows three typical longitudinal MOKE hysteresis loops taken from the as-prepared (100) sample at different in-plane angles φ. The hysteresis loop in figure 1(a) has been recorded at the sample orientation $\varphi = 0°$ (that corresponds to the [010] in-plane direction of the (100) TiO_2 substrate). In this case, we find a rather sharp hysteresis loop with a relatively large coercive field H_c ($\sim$290 Oe), which is typical for a sample magnetically saturated along the easy axis of magnetization. The coercive field reduces slightly for the intermediate angle $\varphi = 45°$ and drops to almost zero ($\leqslant$10 Oe) for $\varphi = 90°$, as can be seen in figures 1(b) and (c), respectively. The shape of the hysteresis loop in figure 1(c) is typical for the magnetic field applied along the hard axis for the magnetization.

The right-hand column in figure 1 shows three longitudinal MOKE hysteresis loops taken from the (001) sample with different in-plane angles φ. The value $\varphi = 0$ corresponds to the [110] in-plane direction of the (001) TiO_2 substrate. A typical easy-axis hysteresis loop with perfect square shape is obtained at $\varphi = 0°$ (figure 1(d)), while the hysteresis loop recorded at an angle $\varphi = 45°$ reveals features expected for the hard-axis direction (figure 1(f)). The coercive field is $\sim$150 Oe for the easy axis, decreasing for the intermediate angle $\varphi = 18°$ (figure 1(e)) and reaching the minimal value of about 25 Oe for the hard-axis angle $\varphi = 45°$.

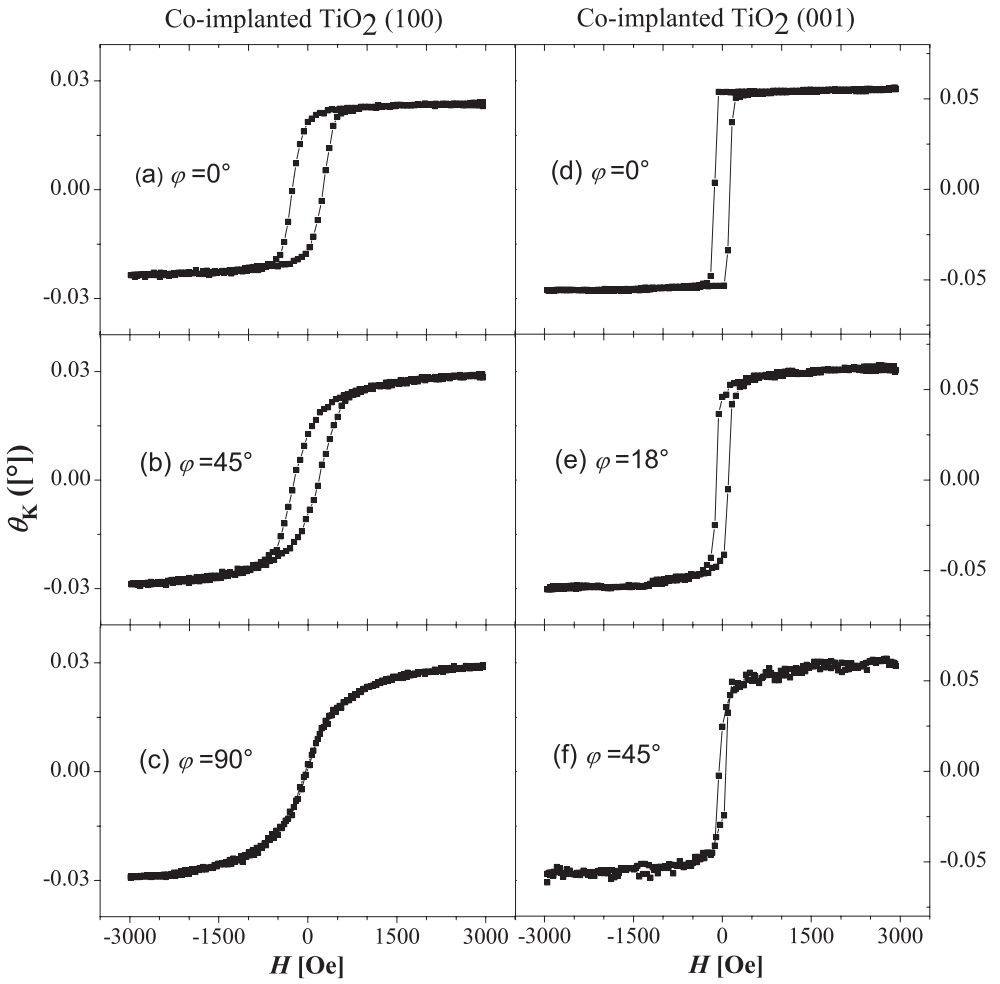

Figure 1. Longitudinal MOKE hysteresis loops, measured at different in-plane angles φ, are presented for the (100) and (001) samples (left and right columns, respectively). Hysteresis loops for the external magnetic field $\boldsymbol{H}$ along the easy-axis ((a) and (d)), intermediate ((b) and (e)) and hard-axis ((c) and (f)) orientations are shown.

The in-plane anisotropy of the hysteresis loops is presented in figures 2 and 3 as a function of the rotation angle φ. Figure 2 shows the remanent Kerr signal θ_K^{rem} normalized to the Kerr signal at saturation θ_K^{sat} as a function of the rotation angle φ for the (100) and (001) samples. According to figure 2(a) the remanent Kerr signal is reduced to almost zero value at the hard-axis orientations, while for the magnetic field applied along the easy-axis orientations (0° and 180°) the ratio $\theta_K^{rem}/\theta_K^{sat}$ is close to unity. Figure 3 shows the coercive field as a function of the angle φ for the (100) and (001) samples. It is clearly visible from figures 2 and 3 that both the remanence signal and the coercive field exhibit dominating twofold symmetry for the (100) sample and dominating fourfold symmetry for the (001) sample.

3.2. SQUID measurements

Hysteresis loops of the Co implanted samples with (100) and (001) orientations, obtained by the SQUID technique, are presented in figures 4 and 5. The loops have been measured

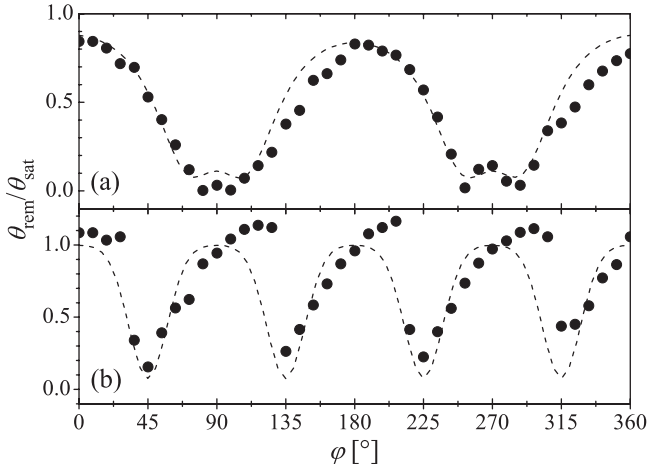

Figure 2. The ratio of the remanence Kerr signal to the saturation signal, $\theta_K^{rem}/\theta_K^{sat}$, as a function of the rotation angle: (a) for the (100) sample, (b) for the (001) sample. The dashed lines are a guide to the eye.

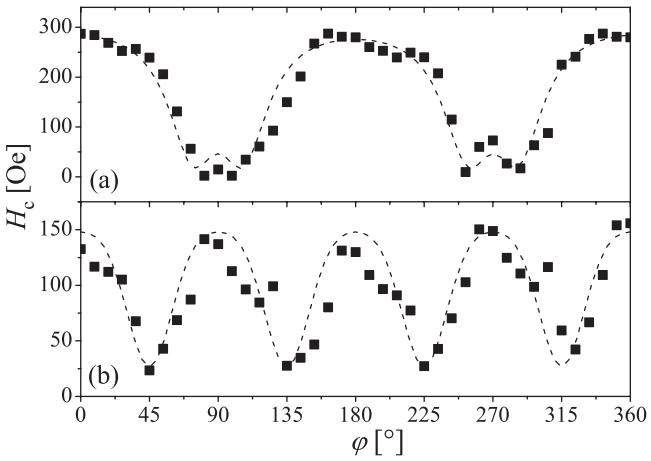

Figure 3. The coercive field H_c as a function of the rotation angle: (a) for the (100) sample and (b) for the (001) sample. The dashed lines are a guide to the eye.

along the easy- and hard-axis orientations determined from the MOKE measurements. The twofold and fourfold behaviour of the in-plane anisotropy have been confirmed by the SQUID hysteresis loops of the (100) and (001) samples, respectively. However, the values of H_c, determined from the SQUID measurements at room temperature, differ noticeably from the MOKE results. We obtained room temperature H_c values of about 105 Oe (50 Oe) along the easy (hard) direction of the (100) sample, and ∼115 Oe (∼60 Oe) along the easy (hard) direction of the (001) sample, respectively. The SQUID measurements also show a striking increase of coercivity for both samples at low temperatures.

4. Discussion

We address the difference in the H_c values obtained by MOKE and SQUID to features of the MOKE technique which probes mainly the in-plane anisotropies of thin layers close to the

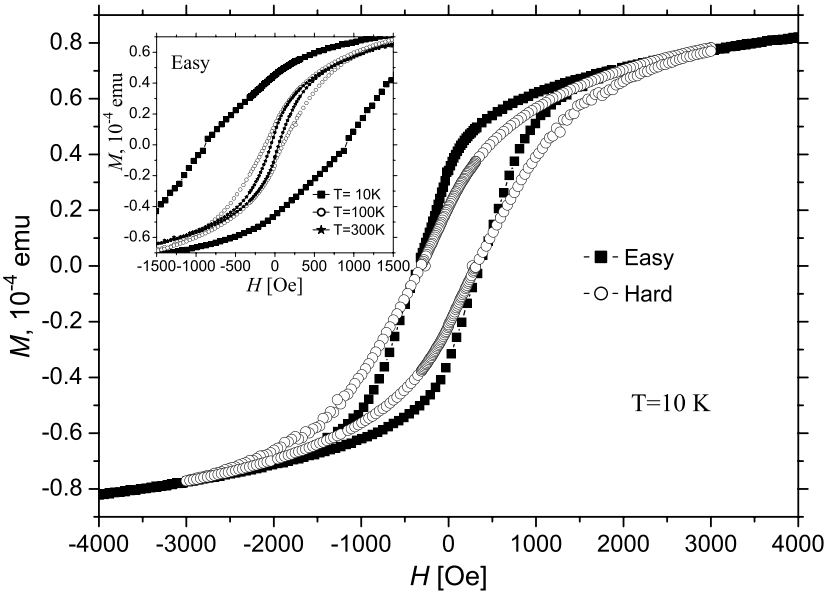

Figure 4. SQUID hysteresis loops for the (100) sample taken at $T = 10$ K along the easy- and hard-axis directions. The inset shows the hysteresis loops measured along the easy axis at various temperatures (10, 100 and 300 K).

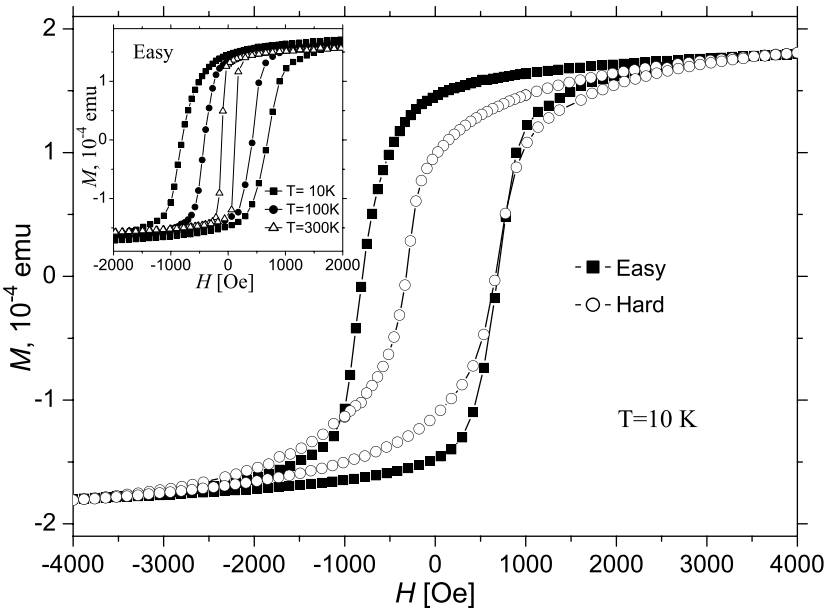

Figure 5. SQUID hysteresis loops for the (001) sample taken at $T = 10$ K along the easy- and hard-axis directions. The inset shows the hysteresis loops measured along the easy axis at various temperatures (10, 100 and 300 K).

surface (∼30 nm). On the other hand, the SQUID technique provides the magnetic properties resulting from the whole ferromagnetic volume of a sample. It is known that the ion-beam synthesis technique results in an inhomogeneous depth profile of the doped ion concentration

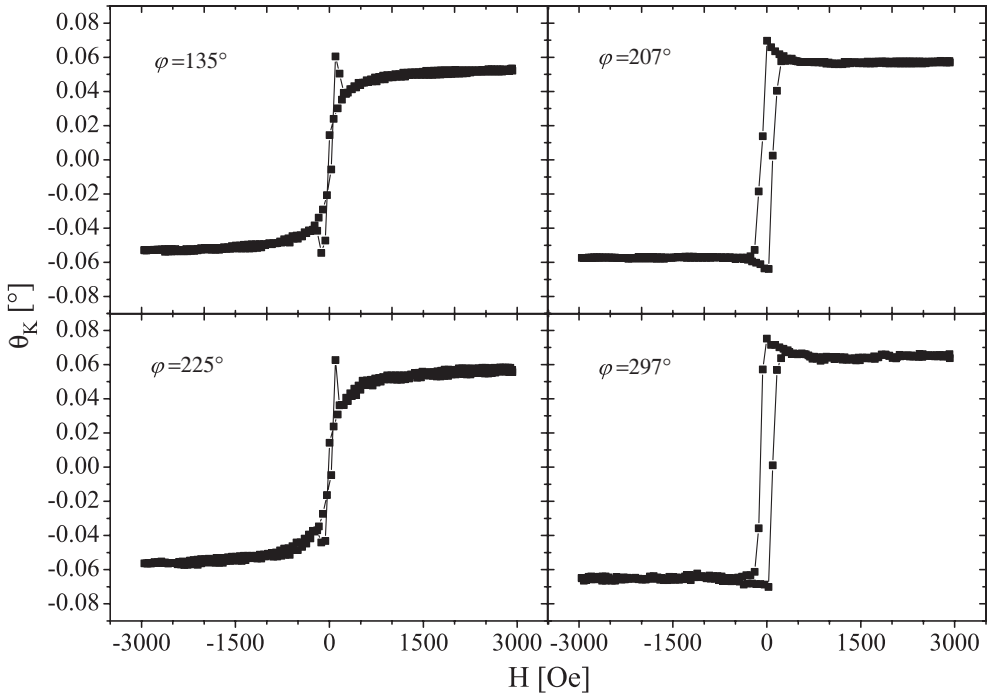

Figure 6. The jumps in the MOKE hysteresis loops, especially pronounced at the angles of $\varphi = 207°$ and 297° (near the hard axis directions) for the (001) sample.

(Co in our case) with a maximum at the depth of about 30 nm. Therefore, the difference between volume and surface magnetic properties may appear as a result of the depth-dependent Co content in the implanted layer. Our FMR studies of the same films [12, 14] revealed a rather broad resonance signal that is an indication of inhomogeneous magnetic properties of the implanted layer.

Another interesting phenomenon observed in the MOKE experiments is the jumps in the hysteresis loops, especially pronounced at some angles near the hard-axis directions for the (001) sample (see figure 6). These non-typical jumps have not been observed in SQUID measurements, hence they are related to the features of the MOKE measurements. In fact, the Kerr-rotation angle θ_K measured in the longitudinal configuration of the MOKE set-up is proportional not only to the longitudinal component of the surface layer magnetization, but also depends on the transverse component of the magnetization, as argued in [15]:

$$\theta_K \propto \cos\theta + \alpha \cos\theta \sin\theta + \beta \sin^2\theta, \tag{1}$$

where $\theta = \varphi_M - \varphi$ is the angle between the magnetization vector and the positive direction of the external field, α and β are parameters which depend on the optic geometry (polarization angle of the incident laser beam, the analyser angle and the incidence angle) and the dielectric tensor of the material [16, 17]. In our case, to obtain magnetic hysteresis loops for various orientations the samples were rotated around the normal to the film plane, while the optic geometry and the magnetic field direction were fixed. Then, the angle changes but parameters α and β remain constant for the different loops. Thus, the Kerr-rotation angle measured in the longitudinal configuration is proportional in first order to the longitudinal component of the magnetization ($\cos\theta$) and in second order to the transverse component of the magnetization given by the terms $\alpha \cos\theta \sin\theta$ and $\beta \sin^2\theta$.

Moreover, it is near the hard axis that the magnetization vector flips from the easy axis to the magnetic field direction. Therefore, the jumps in the MOKE loops, observed at the angles near the hard-axis directions, reflect a considerable contribution of the transverse component due to magnetization reversal near zero field. Another consequence of equation (1) is the fact that the ratio $\theta_K^{rem}/\theta_K^{sat}$ may be larger than unity, which is indeed observed in our MOKE measurements for the Co-implanted (001) TiO_2 sample (figure 2(b)). The second-order effects in the MOKE loops are especially pronounced for the (001) sample that seems to be related to the predominantly fourfold symmetry of the magnetic anisotropy in this sample (figures 2 and 3).

Apart from some quantitative discrepancies, both MOKE and SQUID techniques provide qualitatively similar experimental information on the studied system. It is obvious that the crystallographic orientation of the rutile substrates has a drastic effect on magnetic anisotropy of the implanted layer. Predominantly twofold in-plane anisotropy is observed in the Co-doped (100) TiO_2 sample, while the fourfold anisotropy is revealed in the Co-doped (001) TiO_2 sample (figures 2–5).

In our opinion, two main mechanisms may be relevant for the observed ferromagnetism in the as-implanted Co:TiO_2 system. The first is the formation of a Co nanogranular layer within the irradiated region of rutile. Although we could not detect a cobalt metal nanophase in our XRD measurements, the high value of the effective magnetization revealed in FMR studies [12, 14] indicates a very high cobalt content in the implanted layer. If the observed ferromagnetism is due to the formation of cobalt nanoparticles in the irradiated TiO_2 plates, then the filling factor (f) of metallic cobalt has been estimated to be as high as about 50% [12]. In this case, the in-plane anisotropy observed in our measurements implies a textured growth of the Co nanoparticles in the interior of the supporting tetragonal TiO_2 matrix.

There is also another possibility to explain ferromagnetism in the Co-implanted TiO_2 rutile. Magnetic Co^{2+} ions occupying titanium lattice sites may be strongly exchange coupled via electrons trapped by charge-compensating oxygen vacancies (F-centres). This is the so-called F-centre exchange (FCE) mechanism proposed recently by Coey *et al* [18]. Then, the anisotropy of the dielectric permeability expected from the lattice structure of the rutile substrate could be an additional reason for the anisotropic ferromagnetism in the Co-doped rutile. Experimental techniques, which probe directly the crystalline properties of the irradiated layer and the valence state of the implanted cobalt ions, should be employed to clarify the mechanism of ferromagnetism in the Co:TiO_2 system.

5. Conclusion

The magnetic properties of Co:TiO_2 samples doped by ion implantation have been studied by MOKE and SQUID techniques. The surface magneto-optic response has been probed by the MOKE measurements and has shown low-noise signals of Kerr rotation (magnetization) versus magnetic field. With the SQUID studies we have probed the re-magnetization process of the entire ferromagnetic sample. Both measurements have demonstrated for the first time that the crystallographic orientation of the substrates can be used to tailor magnetic properties of Co-implanted samples; namely, twofold and fourfold in-plane anisotropies have been observed in our MOKE and SQUID studies of the (100) and (001) TiO_2 samples, respectively. Two possibilities for the origin of ferromagnetism in the ion-synthesized Co:TiO_2 system, and accompanying anisotropies have been discussed: formation of metallic cobalt nanoparticles with different textures depending on the crystallographic orientation of the substrate, and the F-centre exchange mechanism.

This work was partially supported by DFG through SFB 491 'Magnetic heterostructures and electronic transport' and by RFBR through grant no. 04-02-97505. N Akdogan acknowledges a fellowship through the International Max-Planck Research School 'SurMat'.

References

[1] Wolf S A, Awschalom D D, Buhrman R A, Daughton J M, von Molnar S, Roukes M L, Chtchelkanova A Y and Treger D M 2001 *Science* **294** 1488
[2] Ohno H, Matsukura F and Ohno F 2002 *JSAP Int.* (N5) 4
[3] Matsukura F, Ohno H and Dietl T 2002 III–V Ferromagnetic semiconductors *Handbook of Magnetic Materials* vol 1, ed K H J Buschow (Amsterdam: Elsevier) p 1
[4] Schmidt G, Ferrand D, Molenkamp L W and van Wees B J 2000 *Phys. Rev.* B **62** R4790
[5] Ueda K, Tabata H and Kawai T 2001 *Appl. Phys. Lett.* **79** 988
[6] Matsumoto Y, Murakami M, Shono T, Hasegawa T, Fukumura T, Kawasaki M, Ahmet P, Chikyow T, Koshihara S and Koinuma H 2001 *Science* **291** 854
[7] Soo Y L, Kioseoglou G, Kim S, Kao Y H, Devi P S, Parise J, Gambino R J and Gouma P I 2002 *Appl. Phys. Lett.* **81** 655
[8] Kim D H, Yang J S, Lee K W, Bu S D, Noha T W, Oh S-J, Kim Y-W, Chung J-S, Tanaka H, Lee H Y and Kawai T 2002 *Appl. Phys. Lett.* **81** 2421
[9] Stampe P A, Kennedy R J, Xin Y and Parker J S 2003 *J. Appl. Phys.* **93** 7864
[10] Punnoose A, Seehra M S, Park W K and Moodera J S 2003 *J. Appl. Phys.* **93** 7867
[11] Rameev B Z, Yildiz F, Tagirov L R, Aktaş B, Park W K and Moodera J S 2003 *J. Magn. Magn. Mater.* **258/259** 361
[12] Khaibullin R I, Tagirov L R, Rameev B Z, Ibragimov Sh Z, Yildiz F and Aktaş B 2004 *J. Phys.: Condens. Matter* **16** L443
[13] Zeidler Th, Schreiber F, Zabel H, Donner W and Metoki N 1996 *Phys. Rev.* B **53** 3256
[14] Aktaş B, Yildiz F, Rameev B Z, Khaibullin R I, Tagirov L and Ozdemir M 2004 *Phys. Status Solidi* c **1** 3319
Aktaş B, Yildiz F, Rameev B Z, Khaibullin R I, Tagirov L and Ozdemir M 2004 *Phys. Status Solidi* c **1** (erratum) (available on-line through the journal WEB site)
[15] Yan S, Schreiber R, Grünberg P and Schäfer R 2000 *J. Magn. Magn. Mater.* **210** 309
[16] Osgood R M III, Clemens B M and White R L 1997 *Phys. Rev.* B **55** 8990
[17] Florczak J M and Dahlberg E D 1990 *J. Appl. Phys.* **67** 7520
[18] Coey J M D, Douvalis A P, Fitzgerald C B and Venkatesan M 2004 *Appl. Phys. Lett.* **84** 1332